

Hierarchical feature extraction on functional brain networks for autism spectrum disorder identification with resting-state fMRI data

Yiqian Luo^a, Qiurong Chen^a, Fali Li^b, Liang Yi^{c,d}, Peng Xu^{a,b,*} and Yangsong Zhang^{a,b,*}

^aLaboratory for Brain Science and Artificial Intelligence, School of Computer Science and Technology, Southwest University of Science and Technology, Mianyang, China

^bMOE Key Laboratory for NeuroInformation, Clinical Hospital of Chengdu Brain Science Institute, and Center for Information in BioMedicine, School of Life Science and Technology, University of Electronic Science and Technology of China, Chengdu, China

^cDepartment of Neurology, Sichuan Provincial People's Hospital, University of Electronic Science and Technology of China, Chengdu, China

^dChinese Academy of Sciences Sichuan Translational Medicine Research Hospital, Chengdu, China

ARTICLE INFO

Keywords:

Autism spectrum disorder
fMRI
Functional connectivity network
Graph convolution
Functional gradients

ABSTRACT

Autism Spectrum Disorder (ASD) is a pervasive developmental disorder of the central nervous system, primarily manifesting in childhood. It is characterized by atypical and repetitive behaviors. Currently, diagnostic methods mainly rely on questionnaire surveys and behavioral observations, which are prone to misdiagnosis due to their subjective nature. With advancements in medical imaging, MR imaging-based diagnostics have emerged as a more objective alternative. In this paper, we propose a Hierarchical Neural Network model for ASD identification, termed ASD-HNet, which hierarchically extracts features from functional brain networks based on resting-state functional magnetic resonance imaging (rs-fMRI) data. This hierarchical approach enhances the extraction of brain representations, improving diagnostic accuracy and aiding in the identification of brain regions associated with ASD. Specifically, features are extracted at three levels: (1) the local region of interest (ROI) scale, (2) the community scale, and (3) the global representation scale. At the ROI scale, graph convolution is employed to transfer features between ROIs. At the community scale, functional gradients are introduced, and a K-Means clustering algorithm is applied to group ROIs with similar functional gradients into communities. Features from ROIs within the same community are then extracted to characterize the communities. At the global representation scale, we extract global features from the whole community-scale brain networks to represent the entire brain. We validate the effectiveness of our method using the publicly available Autism Brain Imaging Data Exchange I (ABIDE-I) dataset. Experimental results demonstrate that ASD-HNet outperforms existing methods. The code is available at <https://github.com/LYQbyte/ASD-HNet>.

1. Introduction

Autism spectrum disorder (ASD) is a type of pervasive developmental disorder affecting the central nervous system (Pandolfi et al., 2018), approximately 1% of the world's population is affected by ASD. Moreover, ASD is associated with a high incidence of concurrent disorders, such as depression and anxiety (Vohra et al., 2017). Autism spectrum disorder typically manifests in childhood, with its associated impairments often persisting throughout an individual's lifetime. Many individuals with ASD require lifelong support to manage their condition (Lord et al., 2018). ASD is characterized by a broad spectrum of symptoms, including deficits in social communication and the presence of restrictive, repetitive behaviors (Hirota and King, 2023; Bhat et al., 2014). The disorder poses significant challenges to both the physical and mental health of affected individuals, profoundly impacting their quality of life as well as that of their families. Despite its profound effects, the precise pathogenesis of ASD remains elusive, making accurate diagnosis particularly challenging.

Unfortunately, there are no definitive drugs and methods for the treatment of ASD, and the pathological mechanisms

of ASD remain for further exploring (Geschwind, 2009). At present, the most effective strategies involve providing advanced behavioral training for individuals with ASD, implementing early intervention programs, and addressing problematic behaviors associated with the condition. These approaches underscore the critical importance of early and accurate diagnosis of ASD. However, relying solely on the manifestation of behavioral symptoms often results in delayed diagnosis, potentially causing patients to miss the optimal window for intervention and complicating treatment efforts. Currently, the majority of diagnostic methods rely on questionnaires and behavioral observations to determine whether an individual has ASD (American Psychiatric Association et al., 2013). These approaches are highly subjective and susceptible to environmental influences, which increases the risk of misdiagnosis (Wang et al., 2022). Consequently, there is an urgent need to develop highly accurate, pathology-based diagnostic tools and to identify reliable biomarkers associated with ASD to improve diagnostic precision and facilitate timely intervention.

Benefiting from the rapid development of medical imaging technology, imaging-based approaches provides us with important tools to analyze and study neurophysiology. Functional magnetic resonance imaging (fMRI), as a non-invasive neuroimaging technique (Matthews and Jezard, 2004), can measure the blood oxygen level dependent

*Corresponding author

✉ xupeng@uestc.edu.cn (P. Xu); zhangysacademy@gmail.com (Y.

Zhang)

ORCID(s):

(BOLD) changes caused by neuronal activity throughout the brain at a series of time points (Friston et al., 1994). Numerous studies have demonstrated the feasibility of utilizing resting-state functional magnetic resonance imaging (rs-fMRI) to investigate the interactions between regions of interest (ROIs) in the brains of individuals with mental disorders (Dvornek et al., 2018). In recent years, a growing body of research has integrated deep learning techniques with rs-fMRI to explore and analyze mental illnesses, achieving notable progress (Dong et al., 2020; Luppi et al., 2022). In most studies, the brain is partitioned into multiple ROIs using predefined brain atlases, followed by the extraction of BOLD time series from these ROIs. Subsequently, the correlations between the BOLD time series of different ROIs are computed to construct brain functional connectivity networks (FCNs), which are then used for further analysis and exploration of brain function (Dong and Sun, 2024; Wang et al., 2023; Hong et al., 2019).

The brain FCN extracted from resting-state fMRI data can reflect the functional interactions between brain regions, which serves as a very effective representation tool to explore the normal and altered brain function (Van Den Heuvel and Pol, 2010). At present, numerous deep learning methods utilize brain FCNs to implement ASD identification. For instance, Eslami et al. proposed using a data-driven linear approach to enhance the training data and using autoencoders to achieve the diagnosis of ASD (Eslami et al., 2019). Kawahara et al. proposed a network architecture called BrainNetCNN, which has special edge-to-edge, edge-to-node, and node-to-graph convolutional filters, and takes into account the non-Euclidean nature of brain networks (Kawahara et al., 2017). Jiang et al. proposed a graph network model Hi-GCN, which first extracts the features of each subject using the ROI-level graph network, and then constructs a population graph network with the extracted features of each subject as nodes (Jiang et al., 2020). Hi-GCN takes into account the spatial properties of brain networks, as well as the structure of the network directly between people. Recently, the DGAIB model proposed by Dong et al. (Dong and Sun, 2024) has utilized graph neural networks to carry out effective feature transmission in brain regions, combining an information bottleneck to filter out irrelevant information related to the target task, thereby applying the retained effective features to improve classification performance. Dong et al. proposed to build an individualized and a common functional connectivity networks, and then use the proposed multiview brain Transformer module to carry out parallel feature extraction learning for the two FCNs (Dong et al., 2024). Finally, the characteristics of the two branches are fused to make the final diagnosis classification.

In recent years, there has been some progress in the research of constructing multi-scale brain network to realize the diagnosis and classification of ASD. For instance, Liu et al. used a set of atlases for multiscale brain parcellation, and then progressively extracted functional connectivity networks from small scale to large scale by constructing mapping relationships between different scale brain maps (Liu

et al., 2023a). Similarly, Bannadabhavi et al. proposed a community-aware approach by using two different scales of atlas and then constructing a map of ROIs to communities based on the division of the two brain atlas (Bannadabhavi et al., 2023). Then transformer (Vaswani et al., 2017) is used to extract ROI-scale network into community-scale brain network for corresponding diagnosis and classification. However, the existing methods all need to manually divide the mapping relationship between ROIs and communities, which is very complicated and cumbersome.

Previous deep learning models often lack the model structure exploration of physiological mechanisms and fail to effectively mine multi-scale features, ranging from local regions to the whole-brain scale, which ultimately leads to suboptimal diagnostic performance. In the current study, we combine resting-state functional magnetic resonance imaging with deep learning techniques to design a network model from a brain physiology perspective, with the goal of improving ASD detection performance. We propose a hybrid neural network model for ASD identification, termed ASD-HNet, which hierarchically extracts features from functional brain networks at three scales: local ROI scale, community scale, and global representation scale. Specifically, we use the Automated Anatomical Labeling (AAL) template (Tzourio-Mazoyer et al., 2002) to divide the brain into N_R ($N_R=116$) regions of interest, extract the BOLD signals from each ROI, and compute the functional connectivity network. A graph convolutional network (GCN) (Niepert et al., 2016) is then employed to transfer information between ROIs. Next, we introduce functional gradients to automatically cluster ROIs into communities, as opposed to relying on pre-defined atlases. This clustering approach groups ROIs with similar functional patterns, allowing us to extract community-scale features. Finally, global brain convolution is applied to the community-scale features to integrate information at the global scale. Additionally, prototype learning is incorporated for classification based on the features extracted by ASD-HNet, leading to improved identification accuracy. Experiments on the publicly available Autism Brain Imaging Data Exchange I (ABIDE-I) dataset validate the superior performance of the proposed ASD-HNet. Moreover, extensive experiments on model generalization further demonstrate the robustness and adaptability of our approach across different datasets.

2. Materials and Methodology

2.1. Functional Gradients

Functional gradients in the brain offer a more comprehensive perspective by capturing the continuous spatial patterns of connectivity beyond the segregated networks typically observed in the human brain (Guell et al., 2018; Huntenburg et al., 2018). It's a gradient-based approach, which performs a nonlinear decomposition of high-dimensional resting-state functional connectivity (rs-FC), can identify distinct brain functional levels by representing connectivity in a continuous, low-dimensional space (Dong

Table 1
Demographic information of subjects from ABIDE-I dataset.

Dataset	Category	Subject	Gender(M/F)	Age(Mean \pm std)
ABIDE-I	ASD	396	347/49	17.78 \pm 9.01
	HC	452	371/81	16.75 \pm 7.25

et al., 2020). Functional gradients have been extensively applied in brain analysis (Dong et al., 2020; Guo et al., 2023; Gong and Zuo, 2023). In the context of various mental disorders, functional gradients provide a clear indication of abnormal functional hierarchies across brain regions.

The functional gradients were also used to study the ASD. For instance, Hong et al. (Hong et al., 2019) found functional gradients disorder in autistic patients, which showed that the functional distances between the transmodal regions and the unimodal regions decreased, that is, the functional independence of the brain region was reduced. Urchs et al. used ABIDE-I dataset (Di Martino et al., 2014) to carry out corresponding functional gradients analysis for autism, and also revealed the compression of gradients (less functional separation) in ASD (Urchs et al., 2022). Although functional gradients has been used in data analysis for ASD, combining functional gradients with deep learning for classification and diagnosis of ASD remain to be explored. In this paper, we proposed a deep learning model by leveraging functional gradients to achieve better ASD identification performance.

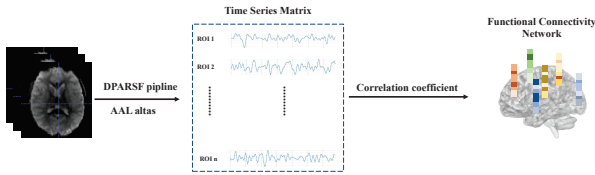


Figure 1: The pipelines process and computation of functional connectivity network.

2.2. Materials and data preprocessing

To verify the performance of the proposed method, we conducted the experiment on the publicly available ABIDE-I dataset, including rs-fMRI and phenotypic data of 1112 subjects from 17 different sites (Di Martino et al., 2014; Craddock et al., 2013). In current study, we utilized rs-fMRI data from 848 subjects, including 396 patients with ASD and 452 health controls (HCs). The demographic information of the studied subjects is reported in Table 1.

For data preprocessing, we used the data Processing Assistant for Resting-State fMRI (DPARSF) to preprocess rs-fMRI data (Yan and Zang, 2010). The specific steps are as follows: (1) Discarding the first 5 volumes. (2) Correcting of slice-related delay. (3) Correcting head movement. (4) Using EPI template normalization in MNI space, resampling to 3 mm resolution of $3 \times 3 \times 3$. (5) Smoothing with a 4 mm full-width at half-maximum (FWHM) Gaussian ker-

nel. (6) Linear detrending and temporal band-pass filtering of BOLD signal (0.01-0.10 Hz). (7) Harmful signals that return head movement parameters, white matter, cerebrospinal fluid (CSF), and global signals. The registered fMRI volumes are then partitioned into N_R ROIs using the AAL template, and BOLD time series are obtained for each ROI. Based on these time series of all the ROIs, we obtained the brain FCN matrix by calculating the Pearson correlation coefficient with the formula (1).

$$\rho_{ij} = \frac{\sum_{t=1}^T (i_t - \bar{i})(j_t - \bar{j})}{\sqrt{\sum_{t=1}^T (i_t - \bar{i})^2} \sqrt{\sum_{t=1}^T (j_t - \bar{j})^2}} \quad (1)$$

Here i_t and j_t ($t = 1, 2, \dots, T$) represent the time series of i -th and j -th brain regions, and the \bar{i} and \bar{j} are the average of two time series of brain region i and j , respectively. T represents the total length of time series.

2.3. Proposed Method

The schematic diagram of the proposed ASD-HNet is shown in Figure 2. This model is designed to progressively extract the discriminative and robust representations based on FCNs from three different scales, i.e., local ROI scale, community scale, and global representation scale, to achieve ASD identification. More details are described below.

2.3.1. The local ROI scale

The suspicious connections calculated with the formula (1) could exist in the FCN, and they can degrade the classification performance of the model using raw FCN as input. To eliminate the influence, we adopted the F -score (Chen and Lin, 2006) as a global feature selector to screen the features in the FCN. For each subject, since their FCN is a real symmetric matrix, we utilized the upper or lower triangle elements of the FCN matrix as the screened features which are then unfolded to a vector. Subsequently, we computed the F -score for each element in the vector by the formula (2).

$$F_i = \frac{(\overline{x_i^{ASD}} - \bar{x}_i)^2 + (\overline{x_i^{HC}} - \bar{x}_i)^2}{\frac{1}{N_{ASD}-1} \sum_{k=1}^{N_{ASD}} (x_{k,i}^{ASD} - \overline{x_i^{ASD}})^2 + \frac{1}{N_{HC}-1} \sum_{k=1}^{N_{HC}} (x_{k,i}^{HC} - \overline{x_i^{HC}})^2} \quad (2)$$

where \bar{x}_i , $\overline{x_i^{ASD}}$, $\overline{x_i^{HC}}$ represent the grand average of the i -th feature of all subjects, the group average of i -th feature of ASD subjects and the i -th feature of HC subjects, respectively. N_{ASD} and N_{HC} denote the number of ASD subjects and HC subjects. The $x_{k,i}^{ASD}$ and $x_{k,i}^{HC}$ refers to the i -th feature of the k -th ASD subject and k -th HC subject, respectively.

Using the F -score, we derived two sparse FCN matrices. Following the methods in (Zhang et al., 2023a; Tong et al.,

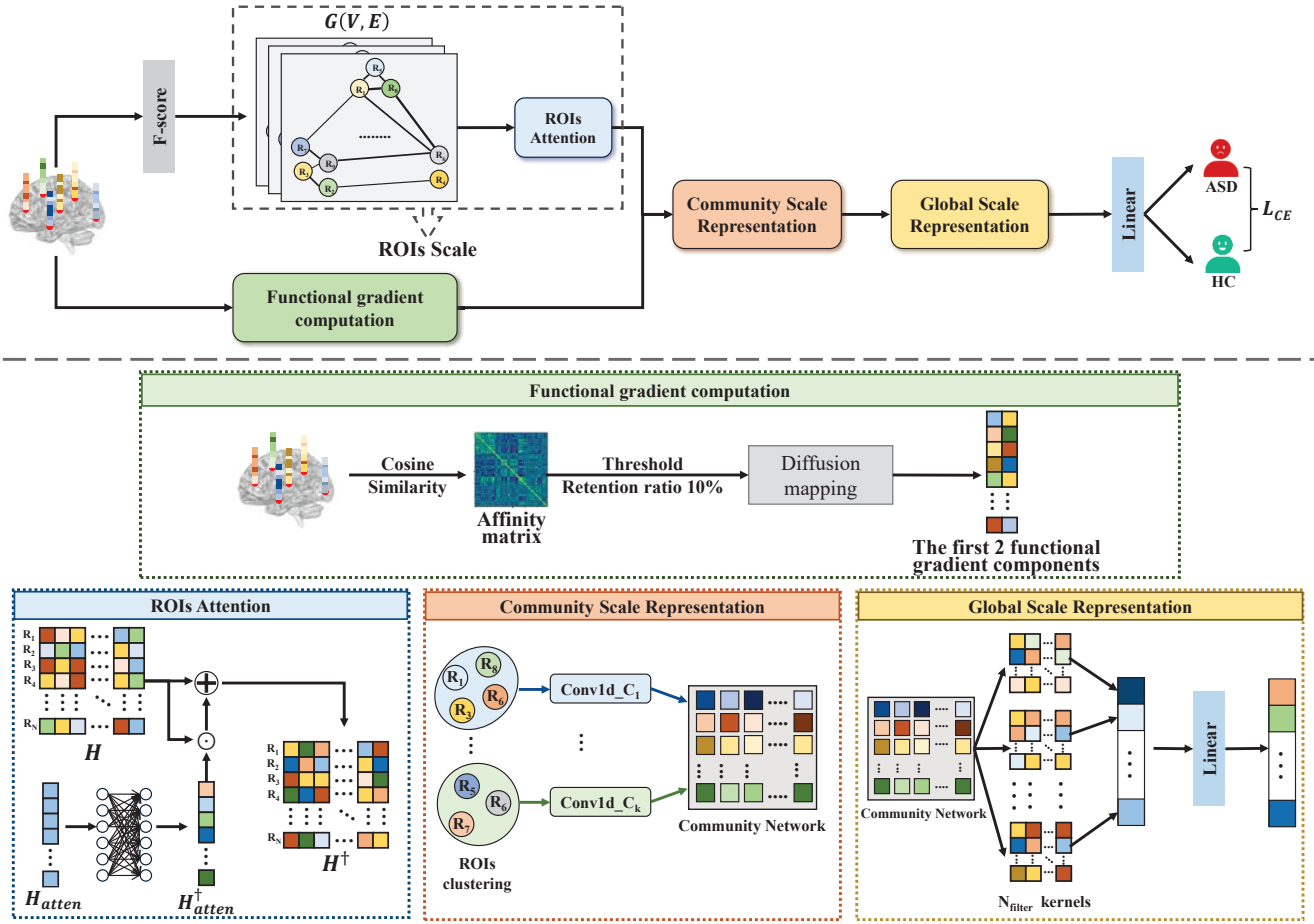


Figure 2: The diagram of the proposed hybrid neural network model for ASD identification (ASD-HNet).

2023), we retained the top 10% of connections in the functional connectivity matrix to construct a sparse FCN matrix, which served as the adjacency matrix (E) for building a graph network. Additionally, to mitigate noise in the node features, we further sparsified the FCN matrix by retaining a proportion λ_R ($\lambda_R=50\%$) based on the F-score criterion.

Based on these two sparse FCN matrices, we constructed a ROI-scale graph network $G(V, E)$, where V is the node feature matrix and E is the adjacency matrix. Then, we used graph convolutional neural network to conduct feature extraction on the ROI scale. Here, we used one layer of spatial-based GCN to complete the message transfer between ROIs, the specific implementation is as follows:

$$H = \sigma(E \cdot V \cdot W) \quad (3)$$

where W is a layer-specific trainable weight matrix with the shape (N_R, D_1) ($D_1=64$) and σ is the activation function. In order to make nodes pay attention to their own characteristics, the diagonal elements of the adjacency matrix E are all set to 1.0.

Following the graph convolution operation, we further employed a ROIs attention mechanism to weight each ROI

features. Specifically, an attention weight matrix H_{atten} was initialized with all elements set to 1.0. Subsequently, two successive fully connected layers were employed to learn the attention weights for each ROI. The operation of a single linear layer is shown in the following formula (4). It should be noted that since ROIs are weighted using positive numbers, so the activation function (σ_{atten}) was ReLU in the fully connected layer.

$$H_{atten}^\dagger = \sigma_{atten} \left(W_{atten}^\dagger H_{atten} + Bias_{atten}^\dagger \right) \quad (4)$$

After obtaining the attention weights of ROIs, we applied these weights to multiply the features of each ROI. Subsequently, a residual connection was employed to integrate the weighted ROI features with the original ROI features, followed by a batch normalization operation, as illustrated in formula (5).

$$H^\dagger = BN \left(H_{atten}^\dagger \odot H + H \right) \quad (5)$$

where BN denotes the BatchNorm1d operation and \odot represents the dot product operation.

2.3.2. The community scale

The brain's community network comprises groups of functionally similar ROIs, each with a high degree of functional concentration. Community networks are crucial for understanding the functional organization of the brain (Van Den Heuvel et al., 2009). Functional communities have been shown to be relevant to understanding cognitive behavior (Van Den Heuvel and Pol, 2010), mental states (Geerligs et al., 2015), and neurological and psychiatric disorders (Canario et al., 2021). We employed the community scale representation module to further extracted functional features at community-clustering scale as illustrated in Figure 2. Since functional gradients can well reflect the functional similarity between ROIs, we proposed to use functional gradients to automatically cluster ROIs into community networks.

We utilized whole group-level (include ASD subjects and HC subjects) average functional connectivity matrix inputs into BrainSpace (Vos de Wael et al., 2020) to obtain group-level functional gradients. In general, the computation of functional gradients involves two steps. The first step is selecting a kernel function to compute the affinity matrix. In the second step, the resulting affinity matrix is subjected to nonlinear dimensionality reduction to obtain the functional gradients. In our work, we chose cosine similarity as the kernel function to compute the affinity matrix ($A(i, j)$). The calculation is expressed as follows:

$$A(i, j) = \cos \text{sim}(R_i, R_j) = \frac{R_i R_j^{Tr}}{\|R_i\| \|R_j\|} \quad (6)$$

where R_i and R_j represent the feature vectors of the i -th and j -th ROI in the FCN, respectively. And $\|\cdot\|$ denotes the l_2 -norm, Tr stands for transpose operation. Before performing the nonlinear dimensionality reduction on the affinity matrix, we first apply sparsification to the matrix. Specifically, we retain only the top 10% (Gong and Zuo, 2023; Vos de Wael et al., 2020) of the strongest functional connections for each ROI, thereby extracting the most significant connections.

For nonlinear dimensionality reduction, we employed the diffusion mapping technique in current study. We calculated the diffusion matrix using the previously obtained affinity matrix $A(i, j)$. The specific calculation process is as follows.

$$P_\beta = D_\beta^{-1} W_\beta \quad (7)$$

where W_β is defined as formula (8), D_β is the degree matrix derived from W_β .

$$W_\beta = D^{-1/\beta} A D^{-1/\beta} \quad (8)$$

where A is the affinity matrix, and D is the degree matrix of A . β is the anisotropic diffusion parameter used by the diffusion operator, whose value is empirically set to 0.5 (Vos de Wael et al., 2020). Then, the eigenvalue decomposition algorithm is used to extract the top n largest eigenvalues (λ)

along with their corresponding eigenvectors (v).

$$P_\beta v = \lambda v \quad (9)$$

Finally, the diffusion embedding is constructed by scaling the eigenvectors to derive the i -th functional gradient component Φ_i .

$$\Phi_i = \frac{\lambda_i}{1 - \lambda_i} \cdot v_i \quad (10)$$

The first N_{gra} ($N_{gra}=2$) components of the functional gradients of each ROI were taken as input, and the unsupervised algorithm K -means was used to complete the clustering of ROIs. In this way, N_R ROIs were clustered into k ($k=7$) communities according to functional similarity. Then we customized a 1D convolution for each community to extract the ROIs features in this community as a representation of this community. The features extraction of each community can be summarized in the following formula.

$$C_i = \sigma(LN(conv1D_i(ROIs_i))) \quad (11)$$

where $ROIs_i$, LN , and σ represent the feature matrix of ROIs belonging to the i -th community, layernorm, and activation function, respectively. And $conv1D_i$ is a one-dimensional convolution operation specific to each community. The parameter settings of the $conv1D_i$ are listed in Table 2.

2.3.3. The global representation scale and classification

By clustering functional gradients and extracting representations of each community, we obtained a functional community network with the shape (k, D_1) . To effectively characterize the brain at a whole-brain scale, we proposed a global scale representation module, which consists of a 2D convolutional layer (with a kernel size equal to the scale of the community network) and a linear layer to achieve whole-brain representation. The parameter details of this module are listed in Table 2.

In order to train the model serving as feature extractor, after the global scale representation module, we used a liner layer and a softmax layer to achieve the supervised classification task (i.e., training process). After the model was trained, we used it as feature extractor (denoted as $f(\cdot)$), the outputs of the global scale representation module were used as the subject's characteristic features.

To implement the classification, the prototype learning was introduced, which achieves classification by learning a set of prototypes, representing the centers of different classes (Qiu et al., 2024). The prototype of the i -th class is computed as follows:

$$P_i = \frac{1}{K} \sum_k f(FC_{k,i}) \quad (12)$$

where P_i ($i = 1, 2$) is the prototype of class i , K represents the number of samples in each class, and $FC_{k,i}$ corresponds to the FCN of the k -th subject in the i -th class.

Table 2
Detailed architecture and parameters of community scale and global representation scale.

Module	Block	Layer	Output size	Explanation
Community Scale	Conv1D _i	Input	(N _i , D ₁)	N _i stands for the number of ROIs belonging to community i, D ₁ =64 outchannel=1, kernel_size=15, padding='same', stride=1
		Conv1d	(1, D ₁)	
		LayerNorm	(1, D ₁)	
		Activation	(1, D ₁)	
		Dropout	(1, D ₁)	
		Concatenate	(k, D ₁)	The features of k communities are concatenated to form a community network
Global Scale	Conv2D	unsqueeze	(1, k, D ₁)	outchannel=16, kernelsize=(k, D ₁), stride=1, D ₂ =16
		Conv2d	(D ₂ , 1, 1)	
		squeeze	(D ₂)	
	Linear	Linear	(D ₂)	in features=D ₂ , out features=D ₂
		Activation	(D ₂)	At this point, we have obtained a feature representation of the whole brain

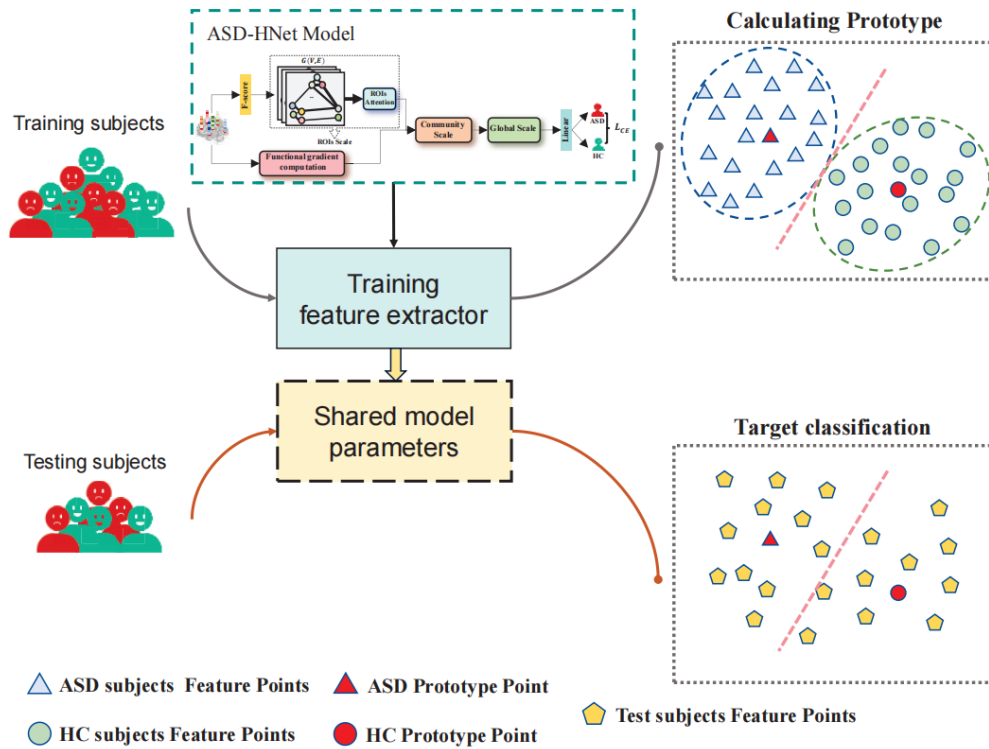


Figure 3: Workflow of prototype learning based classification. First, we use the training set to train the feature extractor, then calculate the corresponding prototype for each category. Finally, we obtain the features of the test data using the trained feature extractor and calculate the distance to each prototype for final classification result.

For the final classification of test subjects, we calculated the Euclidean distance between the feature vectors of the test samples and the two prototypes. Each test sample was then assigned to the class of the prototype with minimal distance, as shown in Figure 3.

2.4. Compared methods

To demonstrate the performance of our proposed method, we compared ASD-HNet with state-of-the-art methods, which are listed as follows.

2.4.1. f-GCN

f-GCN is a basic graph convolutional network. The focus of this method is to choose the appropriate threshold to remove redundant connections, with the optimal threshold

identified in our experiment being 0.1. In f-GCN, multiple GCN layers are stacked. The model employs a global average pooling operator to generate a coarse graph, which reduces the number of parameters by decreasing the size of the representation and thus helps avoid overfitting. The readout layer then consolidates the node representations into a single graph representation (Jiang et al., 2020).

2.4.2. BrainnetCNN

Kawahara et al. proposed a new convolutional model named BrainnetCNN. BrainNetCNN incorporates specific convolutional and pooling layer designs to capture the complex relationships and features within brain networks. Typically, BrainNetCNN includes the following three main components, i.e., Edge-to-Edge (E2E) layer, Edge-to-Node

(E2N) layer, Node-to-Graph (N2G) layer (Kawahara et al., 2017). By combining these layers, BrainNetCNN effectively extracts useful features from brain network data.

2.4.3. CNN-model

Sherkatghanad et al. proposed a two-dimensional convolution of multiple different kernels to extract features at different levels, including features of single ROI and correlation features between ROIs (Sherkatghanad et al., 2020). And then the classification is achieved by fusing the features of different levels. In the end, the convolution with four different kernels performed best on processed data. For simplicity, we termed it as CNN-model, hereafter.

2.4.4. FBNETGEN

FBNETGEN is a learnable method to construct the adjacency matrix and explores the interpretability of the generated brain network for downstream tasks. Specifically, the method uses 1D-CNN and bi-GRU as encoders to learn the features of the time series, and then obtains the learned adjacency matrix by multiplying the learned features with its own transpose. Finally, graph convolution is used to implement the final classification task (Kan et al., 2022a).

2.4.5. ASD-DiagNet

ASD-DiagNet is a collaborative learning strategy that combines single-layer perceptron and autoencoder. For the input data, a linear data enhancement approach is used to augment the training data for better feature extraction (Es-lami et al., 2019).

2.4.6. BrainTransformerNet

BrainTransformerNet leverages transformer to learn the edge attention of functional connectivity and extract an interpretable functional network. In this approach, a new read-out function is also designed to take advantage of modular level similarities between ROIs in the brain network for better brain representation (Kan et al., 2022b).

2.4.7. Hi-GCN

Hi-GCN takes the features of each subject extracted by f-GCN as nodes, and gets the edges between subjects through the calculation of correlation coefficients. After that, the population graph networks is built. Then, four-layer residual graph convolution is used to achieve feature transfer between subjects, and the learned feature representation of each subject is obtained to realize the final classification task (Jiang et al., 2020).

2.4.8. MCG-Net

Luo et al. proposed a dual-branch network architecture, MCG-Net. This method employs parallel convolution and graph convolution to respectively extract high-order representations and low-order spatial features of functional connectivity networks. Ultimately, the extracted multi-features are fused and utilized in a downstream classification task through linear layers. (Luo et al., 2023).

Table 3

Hyper-parameters setting for the proposed model.

	Hyperparameter	Setting
1	Optimizer	Adam
2	Learning rate	0.0001
3	Dropout rate	0.3
4	Training batch size	32
5	Activation function	Tanh(\cdot)
6	Loss	CrossEntropy

2.5. Experimental setting and evaluation metrics

In our experiment, we employed the 10-fold cross-validation strategy to conduct the comparison among different models. The data were divided into 10 folds, with 9 folds used for training and 1 fold used for testing. The models were implemented with PyTorch framework, and all the experiments were conducted on a GeForce RTX 3090 GPU.

We adopted the adaptive moment estimation optimizer (Adam) to train the model with using cross-entropy as the loss function. More hyperparameter settings in the model are listed in Table 3. The cross entropy loss function is defined as below:

$$L_{CE} = \frac{1}{N} \sum_i^N -[y_i \times \log(p_i) + (1 - y_i) \times \log(1 - p_i)] \quad (13)$$

where N denotes the number of training subjects, y_i is the true label of the i -th subject, and p_i stands the predicted probability.

For the hyperparameters N_{gra} and k , we set them to be 2 and 7 during the experiments, respectively. In subsection 3.3.1, we will discuss the influence of different settings on the classification performance.

In order to evaluate the model, four metrics, i.e., sensitivity (Sen), specificity (Spe), accuracy (Acc), and F1, were applied as evaluation indicators. The final values of these metrics were averaged across ten results from 10-fold cross-validation. The definitions were as follows:

$$Acc = \frac{TP + TN}{TP + FN + FP + TN} \quad (14)$$

$$Sen = \frac{TP}{TP + FN} \quad (15)$$

$$Spe = \frac{TN}{TN + FP} \quad (16)$$

$$F1 = \frac{2TP}{2TP + FP + FN} \quad (17)$$

where TP, FN, TN and FP represent the number of ASD subjects correctly classified, the number of ASD subjects wrongly classified as HC subjects, the number of HC subjects correctly classified, the number of HC subjects wrongly classified as ASD subjects, respectively.

Table 4

Performance comparison of among the proposed models and other models. The best results are marked in bold. The results marked with an asterisk (*) are reproduced.

Method	Accuracy(%)	Sensitivity(%)	Specificity(%)	F1-score(%)	p-value
f-GCN*	61.32	61.28	61.31	59.13	0.0002
BrainnetCNN*	64.52	59.84	68.46	61.03	0.0006
CNN-model*	64.88	58.55	69.70	60.36	0.0053
FBNETGEN*	67.14	69.69	64.65	68.59	0.0029
ASD-DiagNet*	66.70	60.64	71.91	62.56	0.0023
BrainTransformerNet*	67.00	64.23	70.23	67.14	0.0151
Hi-GCN*	67.34	68.78	65.70	65.17	0.0052
MCG-Net*	70.48	67.08	73.52	68.32	0.0375
ASD-HNet	73.57	72.63	74.90	71.04	-

3. Results and discussion

3.1. Performance comparison among different methods

The classification results of the ASD-HNet and compared methods are shown in Table 4, with the same experimental settings. All the results of the compared methods were obtained by reproducing the models according to the public codes provided in the references. The hyperparameters were set according to the original studies, except for f-GCN and Hi-GCN. During training the f-GCN and Hi-GCN, we set the corresponding optimal threshold to be 0.1 and 0.2 respectively. It can be found that the proposed ASD-HNet outperforms other methods on all four indicators, with accuracy improved by 3.09%, sensitivity improved by 2.94%, specificity improved by 1.38% and F1-score improved by 2.45%, respectively. To further validate the effectiveness of the proposed method, we performed a paired t-test on the ten-fold cross-validation accuracy of the models. The results reveal that the p-values for comparisons between ASD-HNet and all other methods are less than 0.05, demonstrating the statistical significance of the performance improvements achieved by the proposed method.

To further evaluate the performance of ASD-HNet, we also compared our ASD-HNet method to other four methods that performed well on the ABIDE dataset, i.e., MC-NFE (Wang et al., 2022), MVS-GCN (Wen et al., 2022), MBT (Dong et al., 2024) and DGAIB (Dong and Sun, 2024). In these studies, the authors adopted different amounts of data and different brain templates. Namely, MC-NFE used a total of 609 subjects recruited from 21 sites in ABIDE-I and ABIDE-II (Wang et al., 2022). The MVS-GCN used 871 subjects from 17 different sites, including 403 patients with ASD and 468 normal subjects (Wen et al., 2022). MBT chose 1035 subjects, including 505 patients diagnosed with ASD and 530 healthy controls (Dong et al., 2024). DGAIB pooled 1096 subjects from 17 sites in ABIDE-I, consisting of 569 healthy controls and 527 individuals diagnosed with ASD (Dong and Sun, 2024).

For a intuitive comparison between these method and our ASD-HNet, we directly quoted the reported results from original references as previous studies (Wang et al., 2022). In these studies, the authors did not release the implemen-

tation codes, or did not describe how to generate the used data from ABIDE dataset. The comparison results are summarized in Table 5. By this rough comparison, we can also find that although the F1-score of our method is little lower than MBT and DGAIB methods, our method achieved the best accuracy (73.57%), sensitivity (72.63%) and specificity (74.90%).

3.2. Ablation experiment

To evaluate the rationality and effectiveness of the proposed model's architecture, we conducted a series of ablation experiments to assess the impact of removing each key module on overall performance. Specifically, to validate the effectiveness of information transfer in the ROI-scale graph convolution and to determine whether the ROIs attention module contributes to improved model performance, we performed comparative experiments with and without the graph convolutional network and the ROIs attention mechanism. Additionally, to test the validity of prototype learning, we trained the feature extractor using only the original linear layer for classification, thereby isolating the contribution of prototype learning to the model's performance. The results of the ablation experiment were shown in Table 6.

Through the ablation experiment results, we can find that the performance of the model decreased significantly after the elimination of three modules respectively. Although removing prototype learning decreased the specificity, the proposed model could provide higher sensitivity for effectively diagnosing the ASD subjects, and achieved more balanced performance on the two metrics of sensitivity and specificity.

3.3. The influence of the hyperparameters settings on the model performance

3.3.1. Influence of the N_{gra} and k

In ASD-HNet, two hyperparameters N_{gra} and k need to be configured, which represent the number of functional gradients components and the number of functional communities, respectively. The results reported above were obtained when N_{gra} and k were set to be 2 and 7. Different combinations of these two hyperparameters may lead to varying classification performance. To investigate the impact of hyperparameter settings on model performance, we conducted the systematic hyperparameter search experiments as previ-

Table 5

Comparison with state-of-the-art methods(ABIDE), with best results shown in bold. '-' indicates the experiment results are not reported on the dataset.

Method (ASD/HC)	MC-NFE (Wang et al., 2022) (280/329)	MVS-GCN (Wen et al., 2022) (403/468)	MBT (Dong et al., 2024) (505/530)	DGAIB (Dong and Sun, 2024) (527/569)	ASD-HNet (Ours) (396/452)
Atlas	BASC-064	AAL-116	AAL-116	AAL-90	AAL-116
ACC(%)	68.42	68.92	72.08	71.20	73.57
SEN(%)	70.05	69.09	72.26	69.60	72.63
SPE(%)	63.64	63.15	71.50	73.41	74.90
F1-score(%)	-	-	71.69	71.39	71.04

Table 6

The results of ablation experiments. The best results are marked in bold.

Method	Accuracy(%)	Sensitivity(%)	Specificity(%)	F1-score(%)
w/o ROI-scale GCN	70.12	67.58	72.51	68.13
w/o ROIs attention	71.79	69.85	73.53	70.04
w/o Prototype Learning	72.86	67.83	77.07	69.82
ASD-HNet	73.57	72.63	74.90	71.04

ous studies (Jiang et al., 2020; Wen et al., 2022; Wang et al., 2024). We conducted experiments with k ranging from 5 to 10 and N_{gra} ranging from 2 to 6. The experimental results are illustrated in Figure 4. The highest score for each metric is marked with a red circle.

From the results in the Figure 4, we can find that although the best combination of hyperparameter values in the sensitivity index is different from the other three indicators, the three indicators of accuracy, specificity and F1-score all achieve the best performance when $k=7$ and $N_{gra}=2$. Moreover, sensitivity has the third highest score under this combination of hyperparameter values. In previous study, Gong et al. found that the first two functional gradients can explain the majority of variance in functional networks (Gong and Zuo, 2023). Similarly, Samara et al. also found similar results in their research (Samara et al., 2023). Our experimental results are consistent with previous findings. Based on comprehensive evaluation, we set the k and N_{gra} as 7 and 2 in all our experiments.

3.3.2. Influence of the Node Feature Retention Ratio

In the ROIs scale, there exists a hyperparameter λ_R (node feature retention ratio). To investigate the impact of this parameter on the overall structural performance, we conducted a hyperparameter search experiment. The λ_R ranges from 30% to 60% with a step size of 5%. The experimental results are presented in Figure 5. It can be found that when the retention ratio is set at 50%, the model achieves optimal performance in terms of accuracy, sensitivity, and F1-score, while the specificity metric is only slightly lower than that at the 60% ratio. An appropriate retention ratio enables the model to better learn useful features. When the retention ratio is too low, some features beneficial for classification may be inadvertently removed. Conversely, when the retention ratio is too high, an excessive number of noisy features may be retained. Both scenarios can lead to suboptimal model performance. Therefore, we set λ_R to be 50% in current study

to report the experimental results.

3.4. The interpretability and visualization analysis

In this section, we explore the interpretability of the proposed method and the learned ROIs attention, investigating whether the discriminative features identified are interpretable and consistent with previous findings.

First, we want to check whether the model can find the difference patterns of FCN between ASD subjects and HCs subjects. F-score is a technique for extracting key features based on a data-driven approach. For the analysis of key edges of brain regions, we retained the 10% edges with the highest F-score for retention and visualization, as shown in Figure 6. All the visualization are achieved with Brain-Net Viewer (Xia et al., 2013) tool. The most differentiated edges observed in Figure 6 are mostly the connections between the temporal lobe, the frontal lobe and the sensorimotor area, which is consistent with previous findings. For instance, Abrams et al. has reported an atypical decline in functional connectivity between the temporal area (auditory network) and the medial prefrontal area (DMN) in people with autism (Abrams et al., 2013).

Furthermore, we want to show that the functional gradients in the model can find the difference patterns on the community networks. We conducted the analysis of the validity and interpretability of utilizing the first two components of functional gradients for constructing community networks. Since the gradients calculated separately for the two groups of levels may not be directly comparable (Vos de Wael et al., 2020), we chose the joint embedding (Xu et al., 2020b) to realize the alignment of the two groups of functional gradients. Then we conducted a joint analysis of the principal and secondary gradients.

We merged the first two gradients (principal and secondary gradients) and employed Euclidean distance (consistent with K-Means algorithm) to measure the distinction in corresponding ROIs between the ASD and HC groups.

Hierarchical feature extraction model for ASD classification

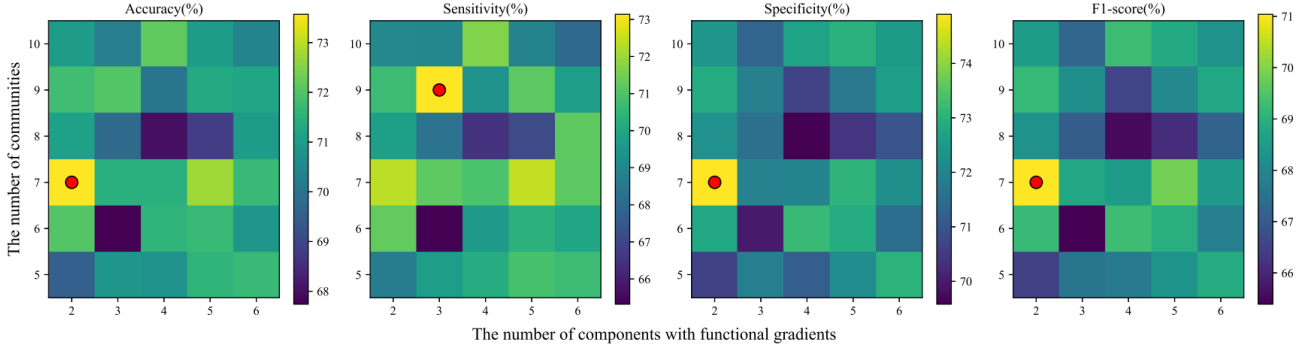


Figure 4: The averaged four metrics obtained by different combination of the parameters k and N_{gra} .

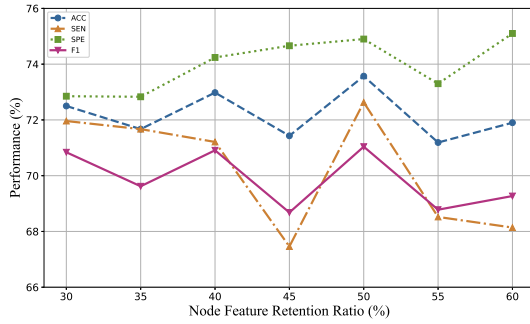


Figure 5: Impact of node feature retention ratio (λ_R) on model performance.

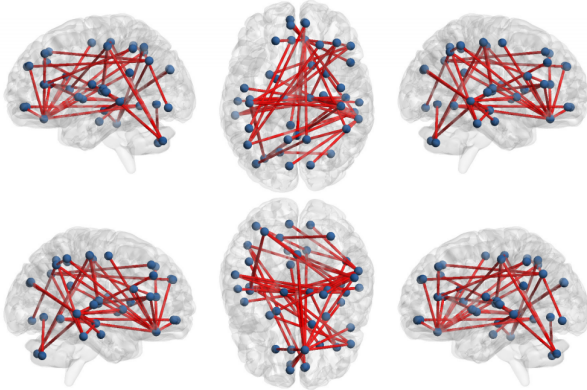


Figure 6: The edges of the brain regions with the greatest difference between HC and ASD patients.

Subsequently, we visualized the ten brain regions with the greatest Euclidean distance (indicating the most significant difference). The visualized result is shown in Figure 7a.

Based on the aforementioned findings, we can observe that the group-level functional gradient differences are primarily reflected in the following brain regions: the inferior orbital gyrus (ORBinf.R), right cerebellar Crus II (CR-

BLCrus2.R), left middle temporal gyrus (MTG.L), left middle frontal gyrus (MFG.L), right hippocampus (HIP.R), right precuneus (PCL.R), right middle temporal gyrus (MTG.R), left middle occipital gyrus (MOG.L), vermis (Vermis45), and right precuneus (PCUN.R). The MTG has been widely confirmed to be associated with ASD (Xu et al., 2020a). And the cerebellum, due to its crucial role in regulating brain function, has significant associations with ASD (Mosconi et al., 2015; Hampson and Blatt, 2015). Xiao et al. also confirmed the association between the precuneus and ASD (Xiao et al., 2023). These key ROIs and their associations are consistent with the findings of (Hong et al., 2019).

Next, we visualize the ROIs attention weights learned by the model. The ten ROIs with the highest attention scores are visualized in Figure 7b. These ROIs include: left cerebellum (Cere3.L, Cere10.L), left dorsal cingulate gyrus (DCG.L), right olfactory cortex (OLF.R), right triangular part of the inferior frontal gyrus (IFGtriang.R), right cerebellum (Cere8.R), right middle orbital gyrus (ORBmid.R), vermis6, right middle temporal gyrus (MTG.R), and left middle frontal gyrus (MFG.L). We observe that several regions overlap between the group-level differences identified by the functional gradient and those highlighted by the ROIs attention scores, particularly in the temporal lobe (Xu et al., 2020a), left prefrontal cortex (Lee et al., 2009), and certain cerebellar areas (Mosconi et al., 2015; Hampson and Blatt, 2015).

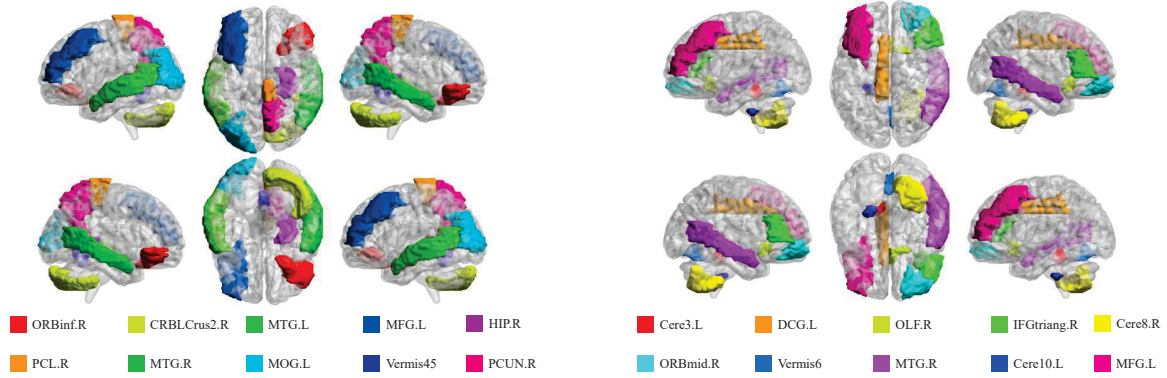
3.5. Experiments on model generalization

In order to investigate the generalization performance of the proposed method, we conducted experiments on both the ADHD-200 Consortium (ADHD-200) dataset¹ and the ABIDE-II dataset (Di Martino et al., 2017).

3.5.1. ADHD-200 Dataset

ADHD-200 dataset has 973 resting state fMRI acquisitions labeled with ADHD or healthy controls from subjects aging from 7 to 21. The dataset is collected from eight different international sites, which are NeuroImage

¹http://fcon_1000.projects.nitrc.org/indi/adhd200/



(a) The ten ROIs with the greatest differences in the first two gradients.

(b) The ten ROIs with the highest attention scores obtained from ROIs attention scores.

Figure 7: The ten ROIs with the greatest differences in the first two functional gradients and the ten ROIs with the most significant differences learned by ROIs attention weights.

group (NeuroImage), New York University Child Study Center (NYU), Peking University (Peking), Brown University (BU), Kennedy Krieger Institute (KKI), University of Pittsburgh (Pitts), Oregon Health and Science University (OHSU) and Washington University in St. Louis (WU).

We choose the dataset preprocessed by Athena pipeline (Bellec et al., 2017). A total of 759 subjects from 7 sites were contained for fMRI data, including 303 ADHD patients and 456 HCs. Similar to the above experiments on ASD, we used 10-fold cross-validation to conduct corresponding experiments. Initially, for ASD-HNet, we used the same hyperparameters as we did for classifying ASD. We then tuned the model based on the specifics of the ADHD data. The adjustments were as follows: (1) Due to the imbalance in the ADHD data, we used a larger batchsize (64) to ensure that each batch included a more balanced representation of both classes. (2) Given the presence of multiple subtypes of ADHD (Molavi et al., 2020), we incorporated more global brain features from different perspectives to enhance the model’s discriminative ability. Specifically, we increased the out_channels of Conv2d in the global brain scale to 32. These adjustments can enhance the model’s adaptation and optimization for classifying ADHD.

In addition to the comparative methods mentioned above for ASD, we also included two state-of-the-art methods in our analysis: (1) MDCN (Yang et al., 2023), which utilize fMRI data from 572 subjects, including 261 ADHD patients and 311 healthy controls (HCs); (2) A-GCL (Zhang et al., 2023b), which uses data from 947 subjects, comprising 362 ADHD patients and 585 HCs. The experimental results are shown in Table 7. The results indicate that our method also achieves better performance in classifying ADHD. Due to the imbalance in the data we used, the comparison methods we reproduced show a significant imbalance in specificity and sensitivity, resulting in a lower F1-score. However, our

method achieves the best performance in terms of accuracy (71.33%) and specificity (80.30%). This demonstrated that ASD-HNet not only performs well in classifying ASD but also achieved good classification performance for ADHD, which validates its robustness and generalization.

3.5.2. ABIDE-II Dataset

The ABIDE-II initiative was established as an extension of ABIDE-I, aiming to further advance scientific research on the brain connectome in Autism Spectrum Disorder. ABIDE-II has aggregated over 1000 additional datasets, offering more comprehensive phenotypic characterizations, particularly in the quantitative assessment of core ASD symptoms and associated features. The project now encompasses 19 research sites, including 10 founding institutions and 7 newly participating members, collectively contributing 1114 datasets from 521 individuals with ASD and 593 healthy controls (age range: 5–64 years). These data were openly released to the global scientific community in June 2016, providing a critical resource for ASD research.

In addition to the ADHD-200 dataset, we also evaluated the generalization performance of ASD-HNet on the ABIDE-II dataset, which consists of fMRI data from individuals with autism spectrum disorder and matched healthy controls. For this dataset, we used data from five sites, i.e., BN, EMC, GU, NYU, and OHSU, including a total of 382 subjects, comprising 185 ASD patients and 197 healthy controls. The preprocessing procedure for this dataset followed the same pipeline as ABIDE-I. Since the sample size of this dataset is smaller than that of the ABIDE-I and ADHD-200 datasets, we employed 5-fold cross-validation to balance training efficiency and validation accuracy. The experimental results are presented in Table 8, five compared methods were selected as the baselines.

The experimental results demonstrate that the ASD-HNet method achieves the best performance, which achieves

Table 7

Experimental results of ASD-HNet on ADHD-200 data, with best results shown in bold. '*' stands that the method has not been reproduced, and the results shown are those reported in the original study and '-' indicates the experiment results are not reported on the dataset. "Tuned" denotes the adjustments made to ASD-HNet through fine-tuning.

ADHD-200	Method	ACC(%)	SEN(%)	SPE(%)	F1-score(%)
	f-GCN	61.12	83.47	27.43	30.95
	BrainnetCNN	62.53	49.64	71.84	51.01
	CNN-model	64.13	43.69	77.64	49.33
	Hi-GCN	66.01	78.96	46.58	51.82
	MCG-Net	68.67	53.30	79.41	57.26
(ADHD/HC)	MDCN* (261/311)	67.45	71.97	62.39	66.86
	A-GCL* (362/585)	70.92	-	-	-
Ours	ASD-HNet	70.00	57.22	78.53	60.44
	ASD-HNet (tuned)	71.33	58.49	80.30	61.80

Table 8

Experimental results of ASD-HNet and compared methods on ABIDE-II data, with the best results are highlighted in bold.

ABIDE-II	Method	ACC(%)	SEN(%)	SPE(%)	F1-score(%)
	f-GCN	62.40	56.20	60.30	52.33
	BrainnetCNN	68.12	69.72	62.12	66.43
	CNN-model	66.85	59.21	70.57	62.49
	Hi-GCN	64.17	64.17	56.58	56.63
	MCG-Net	65.51	61.55	64.06	62.00
	ASD-HNet(ours)	72.55	65.23	78.04	68.75

performance improvements of 4.43% in accuracy, 7.47% in specificity, and 2.32% in F1-score compared to the the second-best method. These additional results further validating the generalization ability of the proposed method across different datasets for the same disease.

3.6. Limitation

Even though ASD-HNet achieved better performance than other methods, some limitations still exist in this study. First of all, the classification performance is still unsatisfactory and can not be applied to clinical scenes in current stage. External cohort datasets should be collected for further validation (Han et al., 2019; Wang et al., 2021). The proposed method relies on a large amount of data for corresponding training. When the amount of data is insufficient or unbalanced, how to maintain the performance of the model is an important issue worthy of further research. Besides, we did not consider the large variability among the dataset from different sites into the model construction in current study. It is beneficial to explicitly eliminate the differences on data distribution with some technologies, such as domain adaption (Wang et al., 2019; Wen et al., 2024; Liu et al., 2023b). We have also recognized the issue of site heterogeneity and have conducted preliminary experiments to mitigate its impact, as discussed in (Luo et al., 2025). In the future, we need address these issues during designing models to conduct the multi-site fMRI data analysis.

4. Conclusion

In this work, we proposed a hybrid neural network model to hierarchically extract features on the functional brain networks for ASD identification. Extensive experiments demonstrate the effectiveness of the proposed model. Compared with other baseline methods, the proposed model achieve superior performance on widely used dataset ABIDE-I. The ablation experiments and the interpretability analysis further verify the rationality of the model architecture. The generalization performance was also explored preliminarily on the ADHD-200 dataset and ABIDE-II dataset. In future studies, it is beneficial to integrate neural mechanisms into the deep learning models to boost the ASD identification.

Acknowledgments

This work was supported in part by the National Natural Science Foundation of China under Grant No.62076209.

CRedit authorship contribution statement

Yiqian Luo: Methodology, Software, Validation, Writing-Original Draft, Writing-Review and Editing, Visualization. **Qirong Chen:** Software, Writing-Review and Editing. **Fali Li:** Methodology, Writing-Review and Editing. **Liang Yi:** Writing-Review and Editing. **Peng Xu:** Conceptualization, Methodology, Writing-Review and Edit-

ing. **Yangsong Zhang**: Supervision, Conceptualization, Methodology, Writing-Review and Editing.

References

- Abrams, D.A., Lynch, C.J., Cheng, K.M., Phillips, J., Supekar, K., Ryali, S., Uddin, L.Q., Menon, V., 2013. Underconnectivity between voice-selective cortex and reward circuitry in children with autism. *Proceedings of the National Academy of Sciences* 110, 12060–12065.
- American Psychiatric Association, D., Association, A.P., et al., 2013. Diagnostic and statistical manual of mental disorders: DSM-5. American psychiatric association Washington, DC.
- Bannadabhavi, A., Lee, S., Deng, W., Ying, R., Li, X., 2023. Community-aware transformer for autism prediction in fmri connectome, in: International Conference on Medical Image Computing and Computer-Assisted Intervention, Springer. pp. 287–297.
- Bellec, P., Chu, C., Chouinard-Decorte, F., Benhajali, Y., Margulies, D.S., Craddock, R.C., 2017. The neuro bureau adhd-200 preprocessed repository. *NeuroImage* 144, 275–286.
- Bhat, S., Acharya, U.R., Adeli, H., Bairy, G.M., Adeli, A., 2014. Automated diagnosis of autism: in search of a mathematical marker. *Reviews in the Neurosciences* 25, 851–861.
- Canario, E., Chen, D., Biswal, B., 2021. A review of resting-state fmri and its use to examine psychiatric disorders. *Psychoradiology* 1, 42–53.
- Chen, Y.W., Lin, C.J., 2006. Combining svms with various feature selection strategies. *Feature extraction: foundations and applications*, 315–324.
- Craddock, C., Benhajali, Y., Chu, C., Chouinard, F., Evans, A., Jakab, A., Khundrakpam, B.S., Lewis, J.D., Li, Q., Milham, M., et al., 2013. The neuro bureau preprocessing initiative: open sharing of preprocessed neuroimaging data and derivatives. *Frontiers in Neuroinformatics* 7, 5.
- Di Martino, A., O’connor, D., Chen, B., Alaerts, K., Anderson, J.S., Assaf, M., Balsters, J.H., Baxter, L., Beggiano, A., Bernaerts, S., et al., 2017. Enhancing studies of the connectome in autism using the autism brain imaging data exchange ii. *Scientific data* 4, 1–15.
- Di Martino, A., Yan, C.G., Li, Q., Denio, E., Castellanos, F.X., Alaerts, K., Anderson, J.S., Assaf, M., Bookheimer, S.Y., Dapretto, M., et al., 2014. The autism brain imaging data exchange: towards a large-scale evaluation of the intrinsic brain architecture in autism. *Molecular psychiatry* 19, 659–667.
- Dong, C., Sun, D., 2024. Brain network classification based on dynamic graph attention information bottleneck. *Computer Methods and Programs in Biomedicine* 243, 107913.
- Dong, D., Luo, C., Guell, X., Wang, Y., He, H., Duan, M., Eickhoff, S.B., Yao, D., 2020. Compression of cerebellar functional gradients in schizophrenia. *Schizophrenia bulletin* 46, 1282–1295.
- Dong, Q., Cai, H., Li, Z., Liu, J., Hu, B., 2024. A multiview brain network transformer fusing individualized information for autism spectrum disorder diagnosis. *IEEE Journal of Biomedical and Health Informatics*, 1–12.
- Dvornek, N.C., Ventola, P., Duncan, J.S., 2018. Combining phenotypic and resting-state fmri data for autism classification with recurrent neural networks, in: 2018 IEEE 15th International Symposium on Biomedical Imaging (ISBI 2018), IEEE. pp. 725–728.
- Eslami, T., Mirjalili, V., Fong, A., Laird, A.R., Saeed, F., 2019. Asd-diagnet: a hybrid learning approach for detection of autism spectrum disorder using fmri data. *Frontiers in neuroinformatics* 13, 70.
- Friston, K.J., Jezzard, P., Turner, R., 1994. Analysis of functional mri time-series. *Human brain mapping* 1, 153–171.
- Geerligs, L., Rubinov, M., Henson, R.N., et al., 2015. State and trait components of functional connectivity: individual differences vary with mental state. *Journal of Neuroscience* 35, 13949–13961.
- Geschwind, D.H., 2009. Advances in autism. *Annual review of medicine* 60, 367–380.
- Gong, Z.Q., Zuo, X.N., 2023. Connectivity gradients in spontaneous brain activity at multiple frequency bands. *Cerebral Cortex* 33, 9718–9728.
- Guell, X., Schmahmann, J.D., Gabrieli, J.D., Ghosh, S.S., 2018. Functional gradients of the cerebellum. *elife* 7, e36652.
- Guo, S., Feng, L., Ding, R., Long, S., Yang, H., Gong, X., Lu, J., Yao, D., 2023. Functional gradients in prefrontal regions and somatomotor networks reflect the effect of music training experience on cognitive aging. *Cerebral Cortex* 33, 7506–7517.
- Hampson, D.R., Blatt, G.J., 2015. Autism spectrum disorders and neuropathology of the cerebellum. *Frontiers in neuroscience* 9, 420.
- Han, S., Wang, Y., Liao, W., Duan, X., Guo, J., Yu, Y., Ye, L., Li, J., Chen, X., Chen, H., 2019. The distinguishing intrinsic brain circuitry in treatment-naïve first-episode schizophrenia: Ensemble learning classification. *Neurocomputing* 365, 44–53.
- Hirota, T., King, B.H., 2023. Autism spectrum disorder: A review. *Jama* 329, 157–168.
- Hong, S.J., Vos de Wael, R., Bethlehem, R.A., Lariviere, S., Paquola, C., Valk, S.L., Milham, M.P., Di Martino, A., Margulies, D.S., Smallwood, J., et al., 2019. Atypical functional connectome hierarchy in autism. *Nature communications* 10, 1022.
- Huntenburg, J.M., Bazin, P.L., Margulies, D.S., 2018. Large-scale gradients in human cortical organization. *Trends in cognitive sciences* 22, 21–31.
- Jiang, H., Cao, P., Xu, M., Yang, J., Zaiane, O., 2020. Hi-gcn: A hierarchical graph convolution network for graph embedding learning of brain network and brain disorders prediction. *Computers in Biology and Medicine* 127, 104096.
- Kan, X., Cui, H., Lukemire, J., Guo, Y., Yang, C., 2022a. Fbnetgen: Task-aware gnn-based fmri analysis via functional brain network generation, in: International Conference on Medical Imaging with Deep Learning, PMLR. pp. 618–637.
- Kan, X., Dai, W., Cui, H., Zhang, Z., Guo, Y., Yang, C., 2022b. Brain network transformer. *Advances in Neural Information Processing Systems* 35, 25586–25599.
- Kawahara, J., Brown, C.J., Miller, S.P., Booth, B.G., Chau, V., Grunau, R.E., Zwicker, J.G., Hamarneh, G., 2017. Brainnetcn: Convolutional neural networks for brain networks; towards predicting neurodevelopment. *NeuroImage* 146, 1038–1049.
- Lee, P.S., Yerys, B.E., Della Rosa, A., Foss-Feig, J., Barnes, K.A., James, J.D., VanMeter, J., Vaidya, C.J., Gaillard, W.D., Kenworthy, L.E., 2009. Functional connectivity of the inferior frontal cortex changes with age in children with autism spectrum disorders: a fmri study of response inhibition. *Cerebral Cortex* 19, 1787–1794.
- Liu, M., Zhang, H., Shi, F., Shen, D., 2023a. Hierarchical graph convolutional network built by multiscale atlases for brain disorder diagnosis using functional connectivity. *IEEE Transactions on Neural Networks and Learning Systems*, 1–13.
- Liu, X., Wu, J., Li, W., Liu, Q., Tian, L., Huang, H., 2023b. Domain adaptation via low rank and class discriminative representation for autism spectrum disorder identification: A multi-site fMRI study. *IEEE Transactions on Neural Systems and Rehabilitation Engineering* 31, 806–817.
- Lord, C., Elsabbagh, M., Baird, G., Veenstra-Vanderweele, J., 2018. Autism spectrum disorder. *The lancet* 392, 508–520.
- Luo, Y., Chen, Q., Zhang, Y., 2025. Multi-site rs-fmri domain alignment for autism spectrum disorder auxiliary diagnosis based on hyperbolic space. URL: <https://arxiv.org/abs/2502.05493>, arXiv:2502.05493.
- Luo, Y., Li, N., Pan, Y., Qiu, W., Xiong, L., Zhang, Y., 2023. Aided diagnosis of autism spectrum disorder based on a mixed neural network model, in: International Conference on Neural Information Processing, Springer. pp. 150–161.
- Luppi, A.I., Mediano, P.A., Rosas, F.E., Holland, N., Fryer, T.D., O’Brien, J.T., Rowe, J.B., Menon, D.K., Bor, D., Stamatakis, E.A., 2022. A synergistic core for human brain evolution and cognition. *Nature Neuroscience* 25, 771–782.
- Matthews, P.M., Jezzard, P., 2004. Functional magnetic resonance imaging. *Journal of Neurology, Neurosurgery & Psychiatry* 75, 6–12.
- Molavi, P., Nadermohammadi, M., Salvat Ghojehbeiglou, H., Vicario, C.M., Nitsche, M.A., Salehinejad, M.A., 2020. Adhd subtype-specific cognitive correlates and association with self-esteem: A quantitative difference. *BMC psychiatry* 20, 1–10.
- Mosconi, M.W., Wang, Z., Schmitt, L.M., Tsai, P., Sweeney, J.A., 2015. The role of cerebellar circuitry alterations in the pathophysiology of autism spectrum disorders. *Frontiers in neuroscience* 9, 156522.

- Niepert, M., Ahmed, M., Kutzkov, K., 2016. Learning convolutional neural networks for graphs, in: International conference on machine learning, PMLR, pp. 2014–2023.
- Pandolfi, V., Magyar, C.I., Dill, C.A., 2018. Screening for autism spectrum disorder in children with down syndrome: An evaluation of the pervasive developmental disorder in mental retardation scale. *Journal of Intellectual & Developmental Disability* 43, 61–72.
- Qiu, L., Li, J., Zhong, L., Feng, W., Zhou, C., Pan, J., 2024. A novel eeg-based parkinson's disease detection model using multiscale convolutional prototype networks. *IEEE Transactions on Instrumentation and Measurement* 73, 1–14.
- Samara, A., Eilbott, J., Margulies, D.S., Xu, T., Vanderwal, T., 2023. Cortical gradients during naturalistic processing are hierarchical and modality-specific. *NeuroImage* 271, 120023.
- Sherkatghanad, Z., Akhondzadeh, M., Salari, S., Zomorodi-Moghadam, M., Abdar, M., Acharya, U.R., Khosrowabadi, R., Salari, V., 2020. Automated detection of autism spectrum disorder using a convolutional neural network. *Frontiers in neuroscience* 13, 482737.
- Tong, W., Li, Y.X., Zhao, X.Y., Chen, Q.Q., Gao, Y.B., Li, P., Wu, E.Q., 2023. fmri-based brain disease diagnosis: a graph network approach. *IEEE Transactions on Medical Robotics and Bionics* 5, 312–322.
- Tzourio-Mazoyer, N., Landeau, B., Papathanassiou, D., Crivello, F., Etard, O., Delcroix, N., Mazoyer, B., Joliot, M., 2002. Automated anatomical labeling of activations in spm using a macroscopic anatomical parcellation of the mni mri single-subject brain. *Neuroimage* 15, 273–289.
- Urchs, S.G., Tam, A., Orban, P., Moreau, C., Benhajali, Y., Nguyen, H.D., Evans, A.C., Bellec, P., 2022. Functional connectivity subtypes associate robustly with asd diagnosis. *Elife* 11, e56257.
- Van Den Heuvel, M.P., Mandl, R.C., Kahn, R.S., Hulshoff Pol, H.E., 2009. Functionally linked resting-state networks reflect the underlying structural connectivity architecture of the human brain. *Human brain mapping* 30, 3127–3141.
- Van Den Heuvel, M.P., Pol, H.E.H., 2010. Exploring the brain network: a review on resting-state fmri functional connectivity. *European neuropsychopharmacology* 20, 519–534.
- Vaswani, A., Shazeer, N., Parmar, N., Uszkoreit, J., Jones, L., Gomez, A.N., Kaiser, L., Polosukhin, I., 2017. Attention is all you need, in: *Advances in neural information processing systems*, pp. 6000–6010.
- Vohra, R., Madhavan, S., Sambamoorthi, U., 2017. Comorbidity prevalence, healthcare utilization, and expenditures of medicaid enrolled adults with autism spectrum disorders. *Autism* 21, 995–1009.
- Vos de Wael, R., Benkarim, O., Paquola, C., Lariviere, S., Royer, J., Tavakol, S., Xu, T., Hong, S.J., Langs, G., Valk, S., et al., 2020. Brainspace: a toolbox for the analysis of macroscale gradients in neuroimaging and connectomics datasets. *Communications biology* 3, 103.
- Wang, J., Wang, X., Wang, R., Duan, X., Chen, H., He, C., Zhai, J., Wu, L., Chen, H., 2021. Atypical resting-state functional connectivity of intra/inter-sensory networks is related to symptom severity in young boys with autism spectrum disorder. *Frontiers in Physiology* 12.
- Wang, M., Zhang, D., Huang, J., Yap, P.T., Shen, D., Liu, M., 2019. Identifying autism spectrum disorder with multi-site fMRI via low-rank domain adaptation. *IEEE Transactions on Medical Imaging* 39, 644–655.
- Wang, N., Yao, D., Ma, L., Liu, M., 2022. Multi-site clustering and nested feature extraction for identifying autism spectrum disorder with resting-state fmri. *Medical image analysis* 75, 102279.
- Wang, Q., Wang, W., Fang, Y., Yap, P.T., Zhu, H., Li, H.J., Qiao, L., Liu, M., 2024. Leveraging brain modularity prior for interpretable representation learning of fmri. *IEEE Transactions on Biomedical Engineering* 71, 2391–2401.
- Wang, Y., Genon, S., Dong, D., Zhou, F., Li, C., Yu, D., Yuan, K., He, Q., Qiu, J., Feng, T., et al., 2023. Covariance patterns between sleep health domains and distributed intrinsic functional connectivity. *Nature Communications* 14, 7133.
- Wen, G., Cao, P., Bao, H., Yang, W., Zheng, T., Zaiane, O., 2022. Mvs-gen: A prior brain structure learning-guided multi-view graph convolution network for autism spectrum disorder diagnosis. *Computers in biology and medicine* 142, 105239.
- Wen, L., Chen, S., Xie, M., Liu, C., Zheng, L., 2024. Training multi-source domain adaptation network by mutual information estimation and minimization. *Neural Networks* 171, 353–361.
- Xia, M., Wang, J., He, Y., 2013. Brainnet viewer: a network visualization tool for human brain connectomics. *PloS one* 8, e68910.
- Xiao, Y., Wen, T.H., Kupis, L., Eyler, L.T., Taluja, V., Troxel, J., Goel, D., Lombardo, M.V., Pierce, K., Courchesne, E., 2023. Atypical functional connectivity of temporal cortex with precuneus and visual regions may be an early-age signature of asd. *Molecular autism* 14, 11.
- Xu, J., Wang, C., Xu, Z., Li, T., Chen, F., Chen, K., Gao, J., Wang, J., Hu, Q., 2020a. Specific functional connectivity patterns of middle temporal gyrus subregions in children and adults with autism spectrum disorder. *Autism Research* 13, 410–422.
- Xu, T., Nanning, K.H., Schwartz, E., Hong, S.J., Vogelstein, J.T., Goulas, A., Fair, D.A., Schroeder, C.E., Margulies, D.S., Smallwood, J., et al., 2020b. Cross-species functional alignment reveals evolutionary hierarchy within the connectome. *Neuroimage* 223, 117346.
- Yan, C., Zang, Y., 2010. Dparsi: a matlab toolbox for "pipeline" data analysis of resting-state fmri. *Frontiers in systems neuroscience* 4, 1377.
- Yang, Y., Ye, C., Ma, T., 2023. A deep connectome learning network using graph convolution for connectome-disease association study. *Neural Networks* 164, 91–104.
- Zhang, J., Feng, F., Han, T., Gong, X., Duan, F., 2023a. Detection of autism spectrum disorder using fmri functional connectivity with feature selection and deep learning. *Cognitive Computation* 15, 1106–1117.
- Zhang, S., Chen, X., Shen, X., Ren, B., Yu, Z., Yang, H., Jiang, X., Shen, D., Zhou, Y., Zhang, X.Y., 2023b. A-gcl: Adversarial graph contrastive learning for fmri analysis to diagnose neurodevelopmental disorders. *Medical Image Analysis* 90, 102932.